energies

MDPI

Article

Pore Structure and Fractal Characteristics of Coal-Measure Sedimentary Rocks Using Nuclear Magnetic Resonance (NMR) and Mercury Intrusion Porosimetry (MIP)

Na Zhang [1,2,†], Shuaidong Wang [1,2,*,†], Xingjian Xun [1,2], Huayao Wang [1,2], Xiaoming Sun [1,2] and Manchao He [1,2]

[1] State Key Laboratory for GeoMechanics and Deep Underground Engineering, Beijing 100083, China
[2] School of Mechanics, Architecture and Civil Engineering, China University of Mining and Technology, Beijing 100083, China
* Correspondence: bqt1900606067@student.cumtb.edu.cn
† These authors contributed equally to this work.

Abstract: Analyzing and mastering the fractal features of coal-measure sedimentary rocks is crucial for accurately describing the pore structure of coalbed methane resources. In this work, mercury intrusion porosimetry (MIP) and nuclear magnetic resonance (NMR) are performed on coal-measure sedimentary rocks (i.e., shale, mudstone, and sandstone) to analyze their pore structure. Pore size distributions (PSDs) and the multifractal dimensions of the investigated samples are discussed. Moreover, multivariable linear regression models of multifractal dimensions are established through a comprehensive analysis of multifractal characteristics. The results show that sandstone (SS-1) and clay rocks are dominated by nanopores of 0.01 to 1 μm, while sandstone (SS-2) is mostly mesopores and macropores in the range of 1 to 10 μm. The fractal characteristics of the investigated rock samples show a prominent multifractal characteristic, in which D_A reflects the surface structure of micropores, while D_S represents the pore structure of macropores. Multifractal dimension is affected by many factors, in which the D_A is greatly influenced by the pore surface features and mineral components and the D_S by average pore diameters. Moreover, multivariate linear regression models of adsorption pore and seepage pore are established, which have a better correlation effect on the multifractal dimension.

Keywords: coal-measure sedimentary rocks; pore structure; mercury intrusion porosimetry (MIP); nuclear magnetic resonance (NMR); multifractal dimensions

Citation: Zhang, N.; Wang, S.; Xun, X.; Wang, H.; Sun, X.; He, M. Pore Structure and Fractal Characteristics of Coal-Measure Sedimentary Rocks Using Nuclear Magnetic Resonance (NMR) and Mercury Intrusion Porosimetry (MIP). *Energies* **2023**, *16*, 3812. https://doi.org/10.3390/en16093812

Academic Editor: Krzysztof Skrzypkowski

Received: 11 April 2023
Revised: 26 April 2023
Accepted: 27 April 2023
Published: 28 April 2023

1. Introduction

Coal-measure sedimentary rocks, i.e., mudstone, shale, and tight sandstone, with low porosity and permeability as well as complex pore structure, are rich in petroleum resources, which has turned into an investigation hotspot in recent years [1]. Poor connectivity and strong heterogeneity of pore-throat structure are tough issues restricting the efficient exploitation of coal-measure sedimentary rocks [2]. Hence, studying and mastering the pore structure features of coal-measure sedimentary rocks play a valuable, guiding role for the safe and efficient exploitation and utilization of mineral resources [3].

According to Loucks's pore size scale [4], pores can be divided into five parts: picopore (<1 nm), nanopore (1 nm–1 μm), micropore (1 μm–62.5 μm), mesopore (62.5 μm–4 mm), and macropore (4 mm–256 mm). In recent years, a series of experimental methods, i.e., gas adsorption experiment (N_2/CO_2) [5–7], X-ray computed tomography (CT) [8–10], field-emission scanning electron microscope (FE-SEM) [11–14], mercury intrusion porosimetry (MIP) [15,16], nuclear magnetic resonance (NMR) [17–22], and NMR cryoporometry (NMRC) [23], have been carried out to explore the micropore structure of common coal-measure sedimentary rocks. However, limited by the testing principles, each of the aforementioned experimental methodologies has certain restrictions. Although micropore structures can be measured

precisely using the gas adsorption technique (N_2/CO_2), the range is relatively narrow. The CO_2 adsorption technique measures over a range of 2 nm, while the N_2 adsorption technique measures over a range of 2–100 nm [14]. Hence, measuring mesopores and macropores with gas adsorption is not possible. SEM experiments and CT imaging technologies can directly observe rock samples [10]. SEM experiments are limited to qualitative analysis of rock samples, whereas CT experiments can perform quantitative analysis and reconstruct rock cores. However, limited by instrument resolution, CT experiments cannot guarantee both resolution and field of view [24]. In the evaluation of the quality of coal-measure sedimentary rocks, MIP measurements can directly obtain the pore structure parameters, i.e., the pore size distributions (PSDs), median, and average pore diameter [15,25,26]. Meanwhile, NMR is used to determine the fluid distribution and pore structure features, including the T_2 distribution, PSD curves, and other physical parameters of reservoir rocks, because it is non-destructive and highly efficient [17,27]. Nowadays, MIP and NMR measurements are extensively used to analyze the pore structure features of coal-measure sedimentary reservoir rocks [15,18,21,26]. Li et al. [28] used a combination of MIP and NMR methods to analyze the pore structure characteristics of coal and verified the accuracy of the measurement results using various methods. Wang et al. [29] analyzed tight oil sandstone's pore structure and fractal characteristics by combining MIP and NMR. Research shows that the combination of NMR and MIP can improve the accuracy of pore structure characterization. The fractal dimension calculated by the NMR T_2 spectrum is practical for rock physical property analysis.

In 1975, the fractal theory was put forward by Mandelbrot to depict the micropore structure of porous media and has been widely used to investigate the pore structure of reservoir rocks, i.e., coals, tight sandstones, and shales [15,23,29–32]. Currently, many scholars have found that the fractal theory can accurately describe pore structure heterogeneity by using N_2-GA, MIP, NMR, and NMRC [33–36]. Due to the limitation in measurement accuracy and calculation theory of a single experimental method, a combination of multiple experimental methods is often used to illustrate the complex geometric features of pore structure. Research shows that the fractal dimensions of pore structures vary significantly with different pore sizes, indicating remarkable multifractal characteristics of reservoir rocks. Meanwhile, the multifractal dimensions are affected considerably by petrophysical properties and mineral composition [37,38]. At present, the calculation and influencing factors of fractal dimension are indistinct because of the complex pore structure characteristics and mineral composition with strong regional differences. In addition, few quantitative studies on the influencing factors of fractal dimensions are based on MIP and NMR.

This study aims to analyze pore structure and fractal characteristics of representative coal-measure sedimentary rocks using MIP and NMR techniques. Meanwhile, multifractal dimensions of MIP and NMR are calculated, and a corresponding multivariate linear regression model is established. Moreover, the relationship between the physical parameters, mineral components, and multifractal dimensions is discussed systematically. The results can provide a basis for reservoir evaluation of coal-measure sedimentary rocks in this research area.

2. Materials and Methods

2.1. Samples

The research area is located in Daqiang and Jiahe Coal Mines, in Liaoning and Jiangsu Provinces, China. Twelve common fine sedimentary rock samples with three lithologies (i.e., shale, mudstone, and sandstone) were collected from the coal-measure strata of the research area. After sampling, rock samples were sealed in self-sealing bags and immediately sealed with wax after being transported to the ground, which were processed into cylindrical cores with a uniform size of 25 mm × 35 mm in the laboratory. The macromorphological characteristics are shown in Table 1.

The density of all the investigated samples was determined based on their dry weights and bulk volume. The water porosity and gas permeability were obtained based on the ISO/WD 19990 [39]. The water porosities (φ) were measured through water saturation

method, and the permeability (K) was determined using a gas permeability testing apparatus by flowing high-purity nitrogen through the rock samples. According to ISO 10370:2014 [40] and ISO 14689:2017 [41], Bruker D8 Discover X-ray diffractometer and Leco CS-230 determinator were used to perform the total organic carbon (TOC) and X-ray diffraction (XRD) measurements. Then, the TOC contents and the mineralogical compositions of all the core samples could be obtained based on the results of TOC and XRD testing. The X-ray fluorescence measurements of the rock samples are shown in Figure 1. In addition, the mineral composition of the rock sample is primarily quartz and clay minerals, with a trace of K-feldspar and Plagioclase. The clay mineral composition is mainly kaolinite, with trace amounts of chlorite, illite, and an illite/smectite mixed layer (I/S).

Table 1. Macromorphological characteristics of the rock samples.

Sample No.	Lithology	Petrographic Characteristics
SS-1	sandstone	Caesious sandstone with good gradation and fine psephicity of grains
SS-2		Grey–white fine sandstone with good gradation of detrital grains
SH-1	shale	Brown laminar shale with noticeable rhyolitic structure
SH-2		Dark-grey laminated silty shale
SH-3		Grey laminated silty shale
SH-4		Brown laminated silty shale
MS-1	mudstone	Gray massive mudstone
MS-2		Gray massive mudstone
MS-3		Yellow–gray massive mudstone
MS-4		Gray massive mudstone
MS-5		Dark-gray massive mudstone
MS-6		Gray massive mudstone

Table 2 lists the TOC contents and the mineralogical compositions of all the core samples.

Table 2. Total organic carbon (TOC) contents and mineralogical compositions of the investigated rock samples [11].

Sample No.	TOC (%)	Minerals (%)				Clay Minerals (%)				
		Clay Minerals	Quartz	K-Feldspar	Plagioclase	Kaolinite	Chlorite	Illite	I/S	%S
SS-1	0.03	30	43	8	19	77	9	4	10	30
SS-2	0.06	12	54	11	17	89	6	3	2	25
SH-1	10.81	26	52	5	13	60	10	7	23	25
SH-2	5.18	34	24	3	6	55	23	11	11	25
SH-3	2.92	43	41	4	12	49	20	9	22	25
SH-4	3.29	25	16	1	2	46	23	13	18	25
MS-1	1.73	55	35	3	7	34	26	14	26	20
MS-2	0.84	49	35	4	12	44	25	12	19	25
MS-3	0.62	42	39	4	12	45	26	10	19	25
MS-4	0.73	50	38	3	9	39	25	13	23	25
MS-5	1.08	47	37	4	12	45	23	13	19	25
MS-6	1.21	44	41	3	12	44	25	12	19	25

2.2. MIP Measurements

MIP is a conventional method to obtain pore structure features. Pore size distribution and some other parameters, including total pore volume/area and average pore diameter, were all determined using MIP tests using AutoPore IV 9500 Porosimeter in this study. According to ISO 15901-1:2016 [42], the investigated samples were measured with mercury injection pressure steps within the scope of 0.5 and 60,000 psia, which corresponds to pore-throat diameters from 3 nm to 36 5 μm. Pore parameters including total pore area

and average pore diameter were obtained based on MIP measurements. Meanwhile, pore radius can be obtained in MIP tests (Equation (1)):

$$P_c = \frac{2\sigma\cos\theta}{r} \quad (1)$$

where P_c, σ, θ, and r refer to the capillary pressure (MPa), the surface tension, the contact angle (°), and the pore radius (μm), respectively.

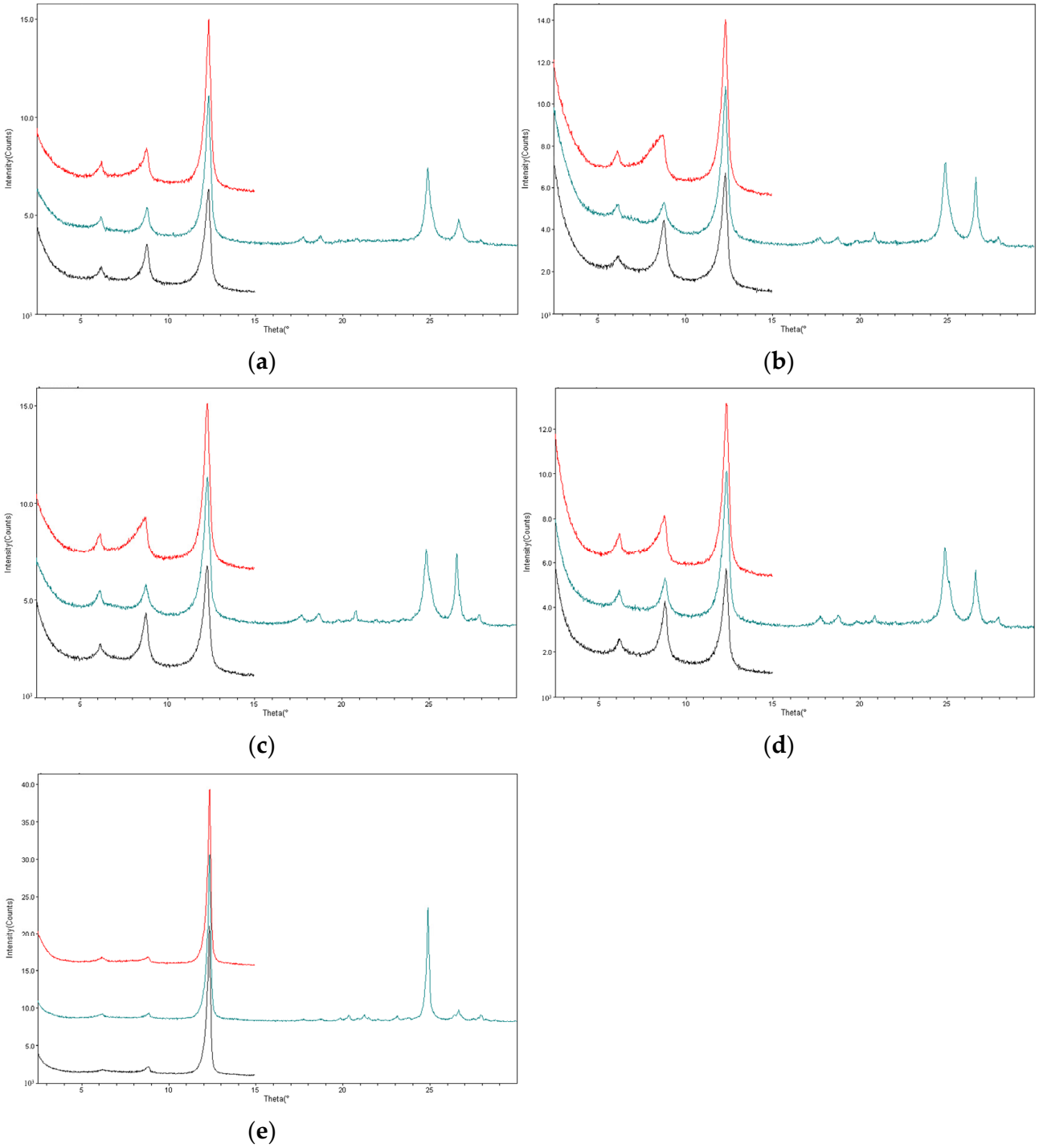

Figure 1. The X-ray fluorescence measurements of the rock samples (**a**) SH-1 clay minerals. (**b**) SH-2 clay minerals. (**c**) MS-1 clay minerals. (**d**) MS-2 clay minerals. (**e**) SS-1 clay minerals [17].

2.3. NMR Measurements

Longitudinal (T_1) and transverse (T_2) relaxation time can provide similar pore distribution information in a low-frequency magnetic field [43], while the T_2 measurement is much faster than the T_1 measurement; hence, the T_2 measurement is often used to obtain pore distribution information [44]. The T_2 cutoff (T_{2c}) determined by the centrifugal calibration method is the critical parameter in NMR tests, which is the threshold to identify the adsorption pore and the seepage pore. Meanwhile, in an external force, the fluid in the seepage pore can flow freely, while in the adsorption pore, it is difficult to flow by the capillary action.

Based on ASTM E2977-14 [45], RecCore-04 NMR sample analyzer was used to perform the NMR tests, with a spectrometer frequency of 3.84 MHz and a constant magnetic field strength of 1200 gauss. The full water-saturated (S_w) samples were measured using NMR measurements at a room temperature of −25 °C to obtain the T_2 spectra. In addition, the test parameters were set as follows: echo spacing, 0.5 ms; waiting time, 3 s; number of echoes, 1024; and number of scans, 64. Pore parameters including porosity and permeability were obtained based on NMR measurements.

3. Results

3.1. TOC and Mineralogical Compositions

As shown in Table 2, the TOC contents are within the scope of 0.03% (SS-1) to 10.81% (SH-1), reflecting the abundance of organic matter. The total organic carbon averages of sandstone, mudstone, and shale are 0.05%, 1.04%, and 5.55%, respectively. Meanwhile, organic matter in clay rocks is significantly more plentiful than that of sandstone. On the one hand, the enrichment of organic matter originates from the input of terrigenous clast. On the other hand, the oxidation–reduction environment plays a vital role in preserving organic matter during diagenetic processes [4,46].

The mineral composition of the investigated rock is dominated by clay minerals and quartz. The main composition of the clay minerals is kaolinite, ranging from 34% (MS-1) to 89% (SS-2), and the average is 37.9%. Among all samples, the quartz content ranges from 16% (SH-4) to 54% (SS-2); the average is 37.9%. Meanwhile, the content of clay mineral averages 38.1%, ranging from 12% (SS-2) to 55% (MS-1). The clay mineral content of mudstone and shale is significantly higher than sandstone, which is between 25% and 55%.

3.2. Petrophysical Properties

As shown in Table 3, the sandstone samples collected from the two coal mines have a massive difference in petrophysical properties. The total porosity and permeability of sandstone are remarkably higher than that of the clay rock samples in the Daqiang Coal Mine. In contrast, rock samples of the Jiahe Coal Mine have similar properties. Among all the rock samples, the porosity range of clay rock samples is 1.40–13.40%, with an average of 7.24%. In addition, low permeability reservoir rocks, i.e., shale and mudstone samples, have poor permeability values, ranging from 0.0003 mD (SH-1) to 0.0048 mD (MS-2). The permeability of SH-2 and MS-3 is significantly lower than that of others with similar porosity because the poor connectivity of the pore structure hinders the fluid flows in the pore throat.

Table 3. Petrophysical properties of the investigated rock samples [11].

Sample No.	Density (g/cm^3)	Total Porosity φ (%)	Permeability K (mD)	Total Pore Area (m^2/g)	Average Pore Diameter (nm)
SS-1	2.57	3.70	0.0046	10.61	10.60
SS-2	2.17	17.50	2.4133	5.20	230.40
SH-1	2.53	1.40	0.0003	10.83	9.5
SH-2	2.64	6.30	0.0006	9.65	11.1
SH-3	2.36	8.20	0.0015	9.18	11.3

Table 3. *Cont.*

Sample No.	Density (g/cm^3)	Total Porosity φ (%)	Permeability K (mD)	Total Pore Area (m^2/g)	Average Pore Diameter (nm)
SH-4	2.51	13.40	0.0028	11.17	10.3
MS-1	2.44	4.70	0.0018	9.62	13
MS-2	2.46	5.80	0.0048	9.42	13.2
MS-3	2.40	6.40	0.0008	8.1	15.6
MS-4	2.40	7.70	0.0017	10.36	13.6
MS-5	2.40	8.30	0.0012	9.75	14.7
MS-6	2.37	10.20	0.0026	8.27	15.8

3.3. Pore Size Distributions (PSDs) Determined by MIP

Pore structure features, i.e., total pore area and average pore diameter determined by MIP tests, are listed in Table 3. The results show that total pore areas are in the range of 1.20 m^2/g (SS-2) to 12.17 m^2/g (SH-4), and the average pore diameters range from 6.7 nm (MS-1) to 230.40 nm (SS-2). The sandstone samples have lower total pore areas with higher average pore diameters than clay rock samples. The average pore diameter of SS-2 is significantly higher than that of the other rock samples, indicating it has stronger pore volumes.

According to the data of the MIP tests, the PSD curves shown in Figure 2 demonstrate the distribution of pore structure. The pore types of experimental samples are dominated by nanopores (r < 1 μm) and micropores (1 μm < r < 62.5 μm). Meanwhile, the pore volumes of the investigated samples are within the scope of 0.0074 mL/g (SH-1) to 0.069 mL/g (SS-2). The PSD curves contain three types. The PSD of most clay rock samples has a similar trend that the total pore volume increases rapidly within the scope of 0.01 μm to 0.1 μm while increasing weak in the rest of the pore size range, which indicates the pore types of rock samples are dominated by nanopores ranging from 0.01 μm to 0.1 μm. Meanwhile, the cumulative pore volume of sandstone samples (SS-2) is significantly larger than that of the others, indicating that SS-2 has the greatest porosity. In addition, the PSD curve of SS-2 increases rapidly in the range of 0.01–10 μm, while it is relatively smooth in other pore sizes, indicating the dominant pore size of SS-2 ranges from 0.01 μm to 10 μm. Moreover, the PSD curves of samples (SS-1 and SH-1) maintain a weak variation range in the full pore size range, only increasing slightly when the pore size is less than 0.1 μm, which indicates that the dominant pore type of SS-1 and SH-1 is a nanopore.

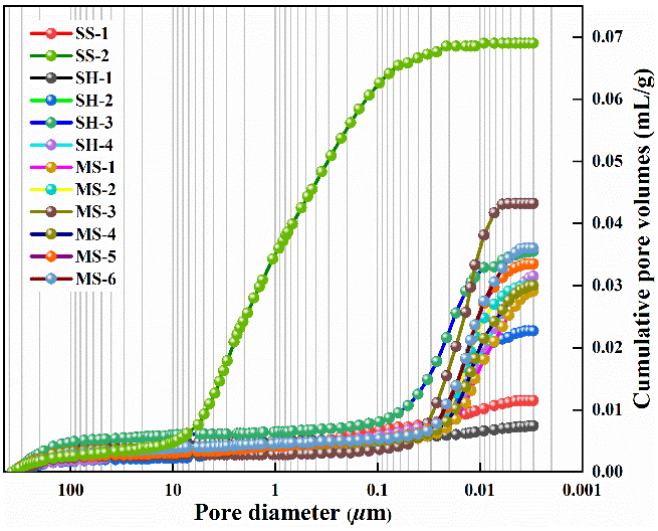

Figure 2. Pore size distribution curves of MIP.

3.4. T_2 Distributions and PSD Determined by NMR

The T_2 distribution is commonly used in the NMR measurement, which is expressed as [43,47]:

$$\frac{1}{T_2} = \frac{1}{T_{2B}} + \frac{1}{T_{2D}} + \frac{1}{T_{2S}} \quad (2)$$

where T_2 is the total transverse NMR relaxation time; T_{2B}, T_{2D}, and T_{2S} are the bulk, diffusion, and surface relaxation time, respectively. The T_2 spectrums of the investigated sample are presented in Figure 3, which depicts the full spectrum pore distributions of the investigated samples. It can be found that the T_2 spectra of all the numbered samples exhibit a single peak distribution, with significant differences in the positions and scales of the peaks. The peak of SS-1 is located at 1 ms, with the prominent peak distributed at 0.1–10 ms, while the peak of SS-2 occurs at 100 ms, with the prominent peak ranging from 1 to 1000 ms. It indicates that SS-1 consists mainly of micropores with a comparatively low pore content, whereas SS-2 predominantly comprises mesopores with an extensive pore size distribution. The peak of the clay rock samples generally appears at 1 ms, with the primary peak distributed between 0.1 and 10 ms, indicating that the clay rock samples consist primarily of micropores. The pore size distribution of the mudstone samples is comparable, as well as the micropore content of the mudstone samples is typically greater than that of the shale samples. Among the shale samples, SH-1 has the highest micropore contents within the range of 0.1–10 ms, whereas the other three samples have comparatively low micropore contents, with a small number of pores greater than 10 ms.

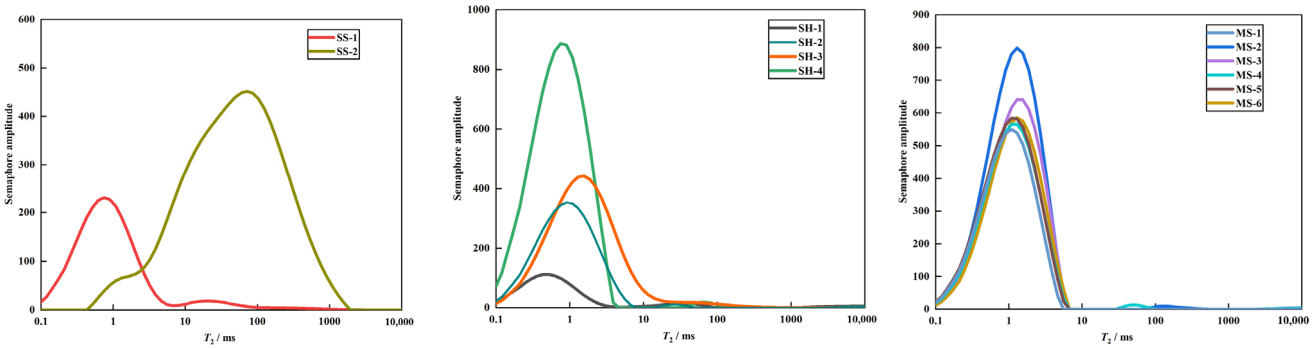

Figure 3. The T_2 distributions of the investigated samples.

On the basis of the principle of NMR measurement [23], the bulk and diffusion relaxation can be ignored, and the T_2 spectra and pore radius, r, show a linear correlation in Equation (3):

$$T_2 = \frac{r}{\rho \times F} \quad (3)$$

where F is the pore shape factor, and r refers to the pore radius, μm.

The quantitative division of adsorption pore and seepage pore is particularly important for reservoir quality evaluation. The fluid in the adsorption pore flows with difficulty due to electrostatic and capillary forces, while the fluid in the seepage pore can flow freely under certain pressure. Commonly, the pore size threshold of adsorption and seepage pores is 0.1 μm [11]. In this study, the analyzed samples' T_2 distributions are converted into PSD curves based on Equation (3). Figure 4 displays the range of pore diameter distribution and the different pore types found in each sample based on the converted PSD curves. As shown in Figure 4 and Table 4, all the PSD curves are unimodal distributions. The peak of sandstone (SS-1), shale, and mudstone are distributed, ranging from 0.01 μm to 1 μm, with the peak points concentrated on about 0.1 μm. The peak area ratios of ≤0.1 μm, 0.1–1 μm, and >1 μm are 38.87–82.14%, 5.20–61.13%, and 0–12.66%, respectively. Moreover the peak area ratio of ≤1 μm is 87.34–100%, indicating that the dominant pore sizes of sandstone (SS-1), mudstone, and shale range from 0.01 to 1 μm and adsorption pores are the dominant

pores. The peak of sandstone (SS-2) is distributed within the scope of 1 μm to 100 μm, with the peak point focused on about 10 μm, and the peak area ratio of >1 μm accounts for 67.92%, indicating that the dominant pore size of sandstone (SS-2) is in the range of 1 μm to 100 μm and seepage pores are the dominant pores.

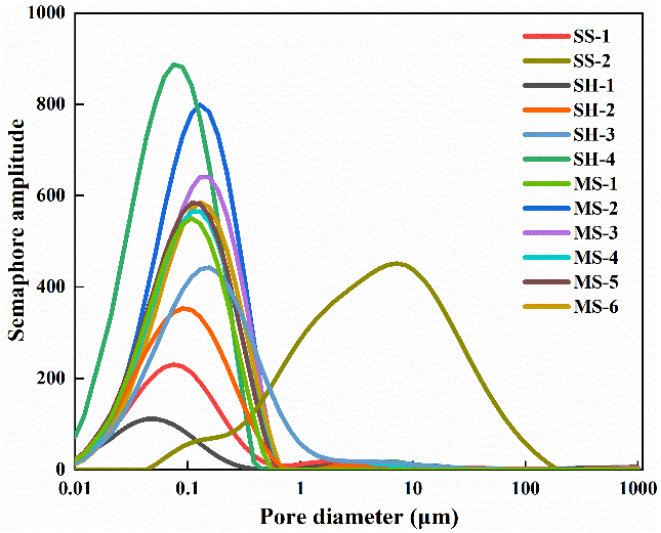

Figure 4. Pore size distribution curves of NMR.

Table 4. Pore size distributions of the investigated rock samples.

Sample No.	Semaphore Amplitude/a.u.					
	Adsorption Pores		Seepage Pores			
	R ≤ 0.1 μm	Proportion/%	0.1 μr < r ≤ 1 μm	Proportion/%	R > 1 μm	Proportion/%
SS-1	1724.89	78.93%	256.98	11.76%	203.38	9.31%
SS-2	127.32	1.11%	3562.99	30.98%	7811.42	67.92%
SH-1	1008.98	82.14%	63.92	5.20%	155.51	12.66%
SH-2	2440.47	53.63%	2047.11	44.99%	62.64	1.38%
SH-3	2208.56	49.31%	1992.96	44.50%	277	6.19%
SH-4	6739.31	56.14%	5166.55	43.04%	98.14	0.82%
MS-1	3167.79	45.49%	3796.23	54.51%	0	0.00%
MS-2	3800.55	77.68%	1033.72	21.13%	58.47	1.20%
MS-3	2947.82	44.62%	3638.8	55.08%	19.36	0.29%
MS-4	3073.61	43.69%	3891.42	55.32%	69.54	0.99%
MS-5	3305.6	48.37%	3528.63	51.63%	0	0.00%
MS-6	2793.11	38.87%	4392.15	61.13%	0	0.00%

3.5. Fractal Dimension Calculated Using MIP

The fractal equation is shown as follows based on the fractal geometry [30]:

$$S_{Hg} = \left[\frac{r}{r_{max}}\right]^{3-D_{MIP}} \quad (4)$$

Equation (4) can be converted as:

$$\lg S_{Hg} = (3 - D_{MIP})\lg r + (D_{MIP} - 3)\lg r_{max} \quad (5)$$

where r; r_{max}; S_{Hg}; and D_{MIP} refer to pore-throat radius, μm; maximum pore-throat radius, μm; cumulative pore volume (<r), %; and fractal dimension, respectively.

Figure 5 shows the double logarithmic relationship of all rock samples between r and S_{Hg}, in which an apparent difference exists in the tangent slope between the two sides of the

experimental sample at r = 0.1 μm. Hence, the curves are divided into two parts, and the multifractal dimensions of the adsorption pore (r < 0.1 μm) and seepage pore (r ≥ 0.1 μm) are calculated. Table 5 shows the correlation effect of multifractal dimensions and that the average correlation coefficients of the adsorption pore and seepage pore are 0.843 and 0.871, respectively. The relationship between D_{MIP} is $D_A < D_f < D_S$, which has prominent multifractal characteristics. The values of D_A (r < 0.1 μm) range from 2.045 (SH-3) to 2.540 (SH-1), with an average of 2.274. Meanwhile, those of D_S (r ≥ 0.1 μm) are between 2.877 (SH-1) and 2.907 (SH-2), with an average of 2.933.

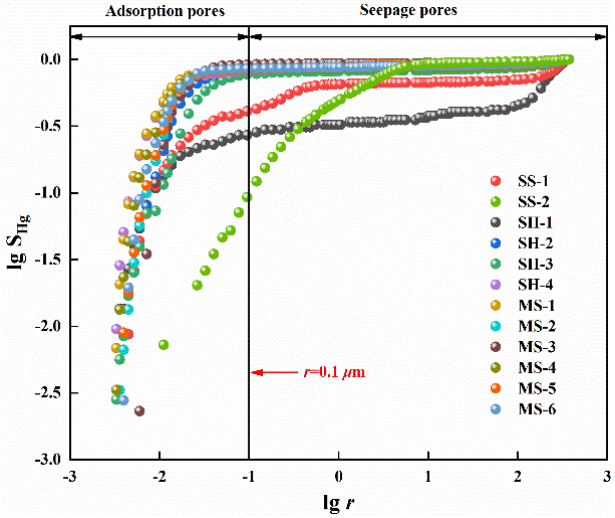

Figure 5. Double logarithmic relationship between r and S_{Hg} of MIP.

Table 5. Calculation results of D_{MIP}.

Sample No.	Porosity φ (%)	Permeability K (mD)	TOC (%)	D_f	Correlation Coefficient	D_A (r ≤ 0.1 μm)	Correlation Coefficient	D_S (r > 0.1 μm)	Correlation Coefficient
SS-1	3.70	0.0046	0.03	2.821	0.391	2.301	0.773	2.966	0.758
SS-2	17.50	2.4133	0.06	2.507	0.766	/	/	/	/
SH-1	1.40	0.0003	10.81	2.771	0.425	2.54	0.563	2.877	0.694
SH-2	6.30	0.0006	5.18	2.793	0.423	2.139	0.871	2.979	0.94
SH-3	8.20	0.0015	2.92	2.724	0.48	2.045	0.913	2.945	0.758
SH-4	13.40	0.0028	3.29	2.663	0.391	2.52	0.841	2.895	0.929
MS-1	4.70	0.0018	1.73	2.764	0.425	2.292	0.877	2.97	0.998
MS-2	5.80	0.0048	0.84	2.682	0.436	2.128	0.889	2.91	0.833
MS-3	6.40	0.0008	0.62	2.725	0.451	2.423	0.887	2.94	0.998
MS-4	7.70	0.0017	0.73	2.753	0.44	2.282	0.889	2.95	0.765
MS-5	8.30	0.0012	1.08	2.762	0.435	2.178	0.888	2.923	0.998
MS-6	10.20	0.0026	1.21	2.683	0.446	2.166	0.88	2.91	0.905

3.6. Fractal Dimension Calculation Using NMR

The total relaxation mechanism of NMR can be simplified as follows [43]:

$$\frac{1}{T_2} \approx \frac{1}{T_{2S}} = \rho\left(\frac{S}{V}\right) = \rho\frac{F_s}{r} \tag{6}$$

where T_{2S} refers to the transverse volume relaxation, ms; ρ refers to the T_2 surface intensity, μm/ms; and F refers to where ρ, F, and r refer to the T_2 surface intensity, μm/ms, the pore shape factor and the pore radius, μm, respectively.

The S_v (cumulative pore volume fraction) can be expressed as:

$$S_v = \frac{V(<r)}{V} = \frac{r^{3-D} - r_{min}^{3-D}}{r_{max}^{3-D} - r_{min}^{3-D}} \tag{7}$$

When $r_{min} << r_{max}$, Equation (7) can be simplified as:

$$S_v = \left(\frac{r}{r_{max}}\right)^{3-D} \tag{8}$$

Then, Equation (8) can be converted as:

$$S_v = \left(\frac{T_{2max}}{T_2}\right)^{D-3} \tag{9}$$

Equation (10) can be expressed as:

$$\lg S_v = (3 - D)\lg T_2 + (D - 3)\lg T_{2max} \tag{10}$$

where T_{2max}, D, and S_V refer to the maximal transverse relaxation, the fractal dimension, and the cumulative pore volume fraction, respectively.

As shown in Figure 6, the double logarithmic relationship of all rock samples between T_2 and S_V, in which an apparent difference exists in the tangent slope between the two sides of the experimental sample at T_2 = 1 ms. Hence, the pore size is divided into two parts: $T_2 < 1$ ms and $T_2 \geq 1$ ms, and the multifractal dimensions of the adsorption pore ($T_2 < 1$ ms) and seepage pore ($T_2 \geq 1$ ms) are calculated, respectively.

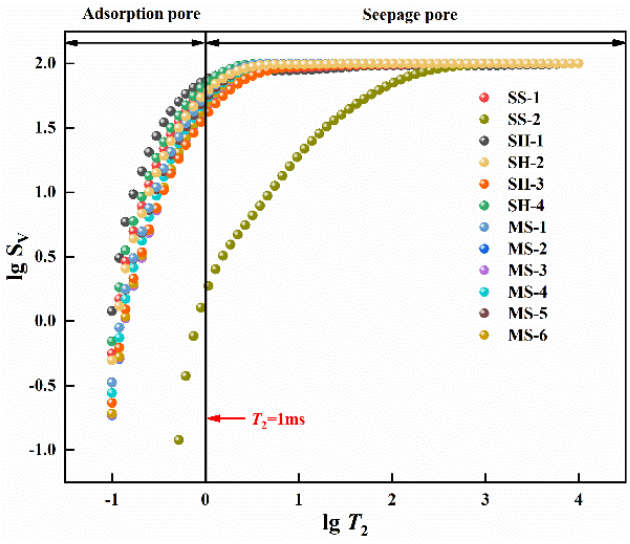

Figure 6. Double logarithmic relationship between T_2 and S_v of NMR.

As shown in Table 6, the D_A is in the range of 2.036 (MS-3) to 2.456 (MS-1), with an average of 2.133. The D_S is between 2.881 (MS-6) and 2.998 (SH-4), with an average of 2.933, denoting the prominent multifractal characteristics of the core samples. Moreover, the relationship of D_{NMR} is D_A (adsorption pore) < D_f (full-size pore) < D_S (seepage pore), Meanwhile, multifractal dimensions are calculated, in which the D_A is close to 2, as well as the D_S is close to 3. This implies that the adsorption pores have good homogeneity, while the seepage pore structure is relatively complex and has strong heterogeneity. Moreover, SS-2 has a wide distribution of the T_2 spectrum with a bit of change in the correlation curve of the full pore size, indicating that the fractal dimension of the sandstone sample SS-2 shows good continuity.

A comparison of the calculated results of D_{MIP} and D_{NMR} is shown in Figure 7. As mentioned above, both D_{MIP} and D_{NMR} exhibit obvious multifractal characteristics, in which the D_A is substantially lower than D_S, demonstrating great homogeneity of adsorption pores. The results of D_{MIP} and D_{NMR} are comparable when calculating the fractal dimension of seepage pores, although the D_A estimated by the MIP experiment is

typically higher than that determined by the NMR experiment. This may be due to the principle of MIP experiments. The measuring aperture and mercury injection pressure in MIP testing are inversely related. The mercury injection pressure used to evaluate the seepage pores is minimal and will not cause damage to the pore structure. However, the pore size of the adsorption pore is typically tiny, and the mercury injection pressure required for measurement is significant. The pore structure will be harmed by the excessive mercury injection pressure, and the pore structure's increased heterogeneity will lead to measurement inaccuracies. The NMR experiment has the characteristic of being non-destructive, so the results are fairly precise when determining the adsorption pore's size.

Table 6. Calculation results of D_{NMR}.

Sample No.	Porosity φ (%)	Permeability K (mD)	TOC (%)	D_f	Correlation Coefficient	D_A ($T_2 \leq 1$ ms)	Correlation Coefficient	D_S ($T_2 > 1$ ms)	Correlation Coefficient
SS-1	3.70	0.0046	0.03	2.795	0.425	2.235	0.84	2.988	0.812
SS-2	17.50	2.4133	0.06	2.507	0.766	/	/	/	/
SH-1	1.40	0.0003	10.81	2.834	0.391	2.456	0.773	2.985	0.817
SH-2	6.30	0.0006	5.18	2.786	0.423	2.165	0.871	2.997	0.45
SH-3	8.20	0.0015	2.92	2.724	0.48	2.041	0.913	2.986	0.509
SH-4	13.40	0.0028	3.29	2.811	0.391	2.256	0.841	2.998	0.794
MS-1	4.70	0.0018	1.73	2.764	0.425	2.048	0.877	2.955	0.793
MS-2	5.80	0.0048	0.84	2.728	0.436	2.056	0.889	2.998	0.33
MS-3	6.40	0.0008	0.62	2.725	0.451	2.036	0.887	2.879	0.905
MS-4	7.70	0.0017	0.73	2.75	0.44	2.078	0.889	2.997	0.41
MS-5	8.30	0.0012	1.08	2.76	0.435	2.041	0.888	2.923	0.89
MS-6	10.20	0.0026	1.21	2.729	0.446	2.053	0.88	2.881	0.88

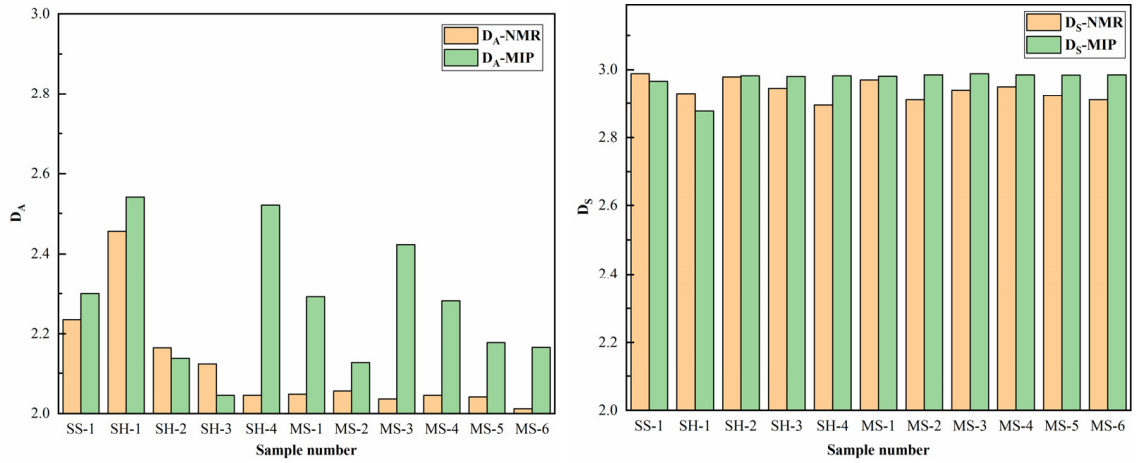

Figure 7. Comparative analysis of D_{MIP} and D_{NMR}.

4. Discussion

The experimental rock samples present apparent multifractal characteristics on the basis of the calculation results of fractal dimensions. This section analyzes the influencing factors of the multifractal dimensions of 10 clay rock samples. Because the MIP experiment is affected by the mercury inlet pressure when measuring micropores, this section selects the D_{NMR} for discussion [23].

4.1. Correlation between Physical Properties and Multifractal Dimensions

To explore the role of physical properties on the fractal features of the experiment samples, the correlation between multifractal dimensions, and the total pore area, the average pore diameter is plotted in Figure 8.

As can be observed, the numbered samples possess remarkable multifractal characteristics, which are affected considerably by petrophysical properties. The D_f, D_A, D_S, and total pore area show a positive correlation, and the correlation coefficients are 0.687, 0.675,

and 0.511, respectively. The relationship of multifractal dimensions is $D_A < D_S$, indicating that the seepage pore has a more heterogonous pore structure. Meanwhile, both D_A and D_S increase with increasing total pore area, which may be due to the fact that the change in the pore space and specific surface area leads to the rise in the heterogeneity of the pore structure [48]. The correlation of D_A with the total pore area is better than that of D_S with the total pore area, which is consistent with previous studies [19,23,49]. For adsorption pores, D_A mainly reflects the surface structure of micropores, greatly influenced by the roughness and specific surface area of the pore surface.

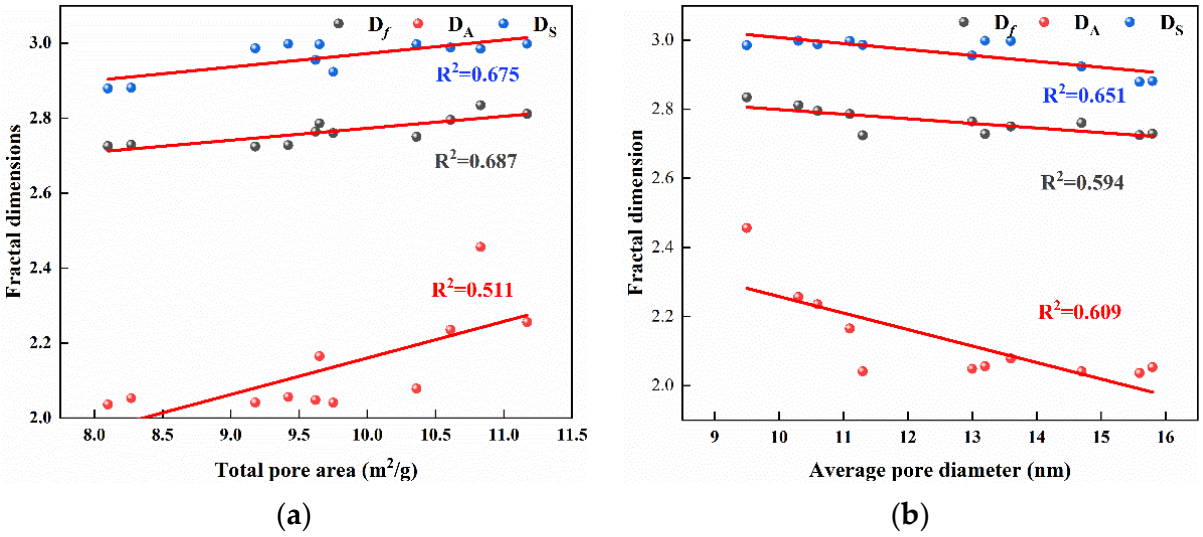

Figure 8. Correlations between (**a**) total pore area, (**b**) average pore diameter, and multifractal dimensions.

Additionally, the D_f, D_A, and D_S negatively correlate with the average pore diameter, with correlation coefficients of 0.597, 0.609, and 0.651, respectively. Both D_A and D_S increase with decreasing average pore diameters, indicating that rock samples with tiny average pore diameters may comprise more throats and micropores, resulting in increasing heterogeneity and more complex pore structures. The D_S shows a better correlation with average pore diameters than D_A. For seepage pores, D_S may best depict the pore structure fractal dimension, which is more susceptible to the average pore diameter than D_A. Multifractal dimensions can better characterize the heterogeneity of rock samples, in which D_A reflects the surface structure of micropores, while D_S represents the pore structure of macropores.

4.2. Correlation between Minerals and Multifractal Dimensions

The correlations between the multifractal dimensions and the TOC content, clay minerals, quartz, chlorite, and illite are shown in Figure 9. The D_f and D_A positively correlate with TOC content with correlation coefficients of 0.646 and 0.845, respectively, whereas the D_S inconspicuously correlates with TOC content. TOC content reflects the abundance of organic matter. Rock samples with high TOC content have more micropores, which leads to a more complex pore structure of adsorption pores, resulting in an increase in D_A [50].

Due to the interaction of multiple factors, i.e., depositional environment, pore type, and the type and content of mineralogical compositions, different mineralogical compositions have diverse mechanical properties and chemical stability, which have various effects on the fractal dimensions. The content of quartz and kaolinite have no apparent correlation with fractal dimensions for some reason, whereas the content of the clay mineral composition shows a negative correlation with the D_f and D_A but an inconspicuous correlation with D_S. Moreover, the content of chlorite and illite shows no apparent correlation with D_f and D_S but a negative correlation with D_A. Clay minerals, including chlorite and illite, mainly contained in the adsorption pores with relatively small pore sizes, are the main

factors affecting the pore structure of reservoir rocks. Hence, the influence of clay mineral composition on the adsorption pores is significant. After reacting with the fluid, the surface of the clay minerals becomes uniform, and the pore heterogeneity is weakened, leading to a decrease in fractal dimensions.

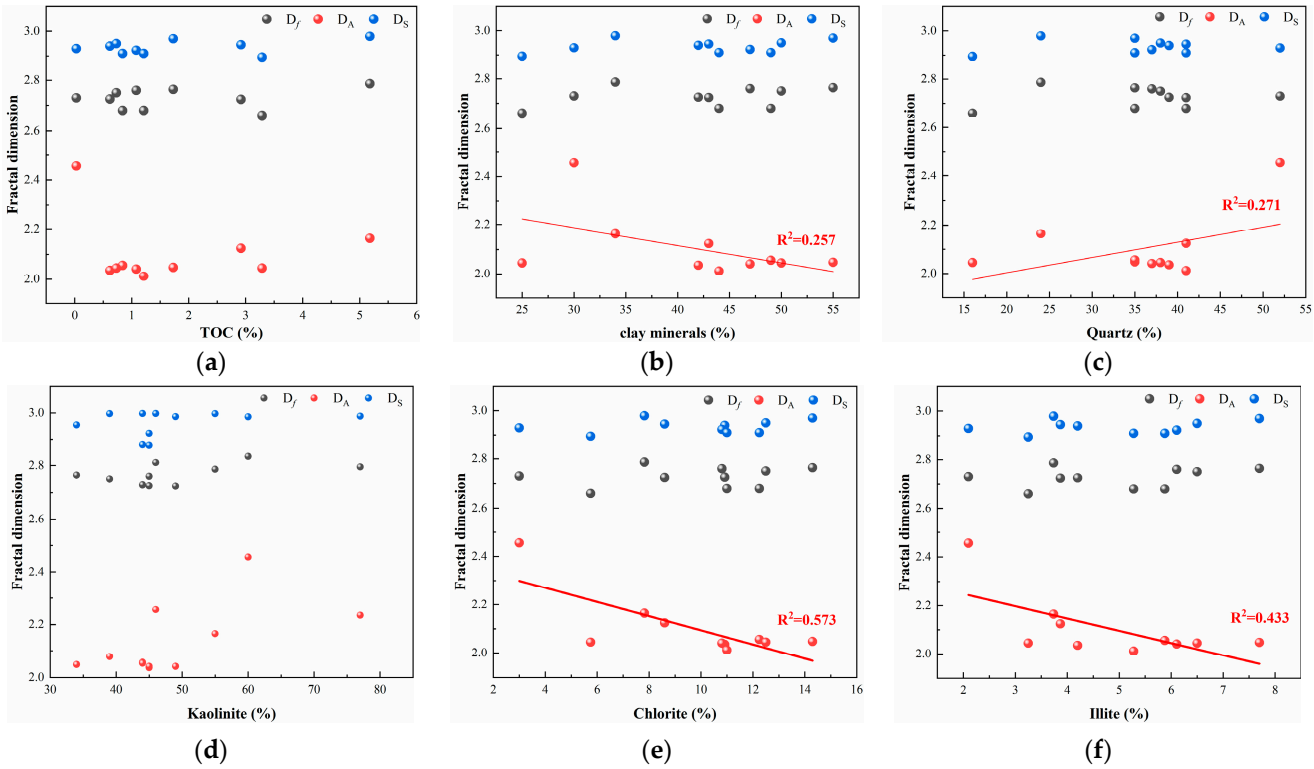

Figure 9. Correlations between the content of (**a**) TOC content, (**b**) clay minerals, (**c**) quartz, (**d**) kaolinite, (**e**) chlorite, (**f**) illite, and multifractal dimensions.

4.3. Fractal Dimension Mathematical Model

As shown in Figures 3 and 4, the experimental samples exhibit prominent multifractal characteristics. The multifractal dimensions are affected by many factors with complex mechanisms. In this paper, the mechanism of action is simplified in order to quantitatively study the effects of various factors on the multifractal dimension. It is assumed that each linearly independent factor linearly correlates with the fractal dimension. Based on correlation analysis, total pore area, and average pore diameter, the content of TOC and clay minerals are selected as the main factor affecting multifractal dimensions. A multivariate linear regression analysis of fractal dimensions was carried out using SPSS, a statistical software for multivariate statistics, to establish the corresponding multivariable linear regression model.

(1) The multivariable linear regression model is established as Equation (11):

$$D = a + bS + cr + d_1C_T + d_2C_C \quad (11)$$

where D is the multifractal dimension; a is const; b, c, d_1, and d_2 are the weighting factors of total pore area, average pore diameter, and the content of TOC and clay minerals, respectively; S is the total pore area; r is the average pore diameter; and C_T and C_C are the absolute content ratios of TOC and clay minerals, respectively.

(2) Entering the parameters after the standardization process, a multivariate linear regression analysis of multifractal dimensions was conducted using SPSS to establish the corresponding multivariable linear regression model, which is shown in Table 7.

Table 7. Parameters of multivariable linear regression models.

Model	R^2	F	a	S		r		TOC		Clay Minerals	
				Beta	t	Beta	t	Beta	t	Beta	t
D_A	0.981	31.454	1.648	0.413	2.877	0.274	1.530	0.578	3.642	−0.390	−2.906
D_S	0.933	8.371	3.148	0.282	1.068	−1.154	−3.491	−0.474	−1.622	0.302	1.221

The parameters of the multivariable linear regression models are presented in Table 6, in which R^2 is the correlation coefficient, F is the statistical value of F-test, and a is const. In this section, ten rock samples from the Daqiang Coal Mine are selected for analysis, and the relationship between the total pore area, average pore diameter, TOC content, clay mineral content, and multifractal dimensions is discussed. Therefore, the number of samples and independent variables is 10 and 4, respectively. Moreover, the degree of freedom is determined by the number of samples and independent variables, and 0.05 is selected as the level of significance in a significance test.

(1) Firstly, the significance test of the whole regression model should be conducted before the significance test of each regression coefficient, which is the joint hypotheses test (F-test). The F-test is used to determine whether the model has a regression relationship. After determining the number of independent variables, degrees of freedom, and the level of a significance test, the critical value of the F-test can be obtained by the critical table, in which $F_{0.05}(4,5) = 5.192$. When $|F| \geq |F_{0.05}(4,5)|$, there is a linear regression relationship between influence factors and multifractal dimensions. Moreover, it can be found that there is a linear regression relationship between D_f, D_A, D_S, and influence factors.

(2) Secondly, a Student's t-test (t-test) is carried out on the model parameters of each factor to judge the significance of each independent variable to the dependent variable, of which the degree of freedom and the level of a significance test are 5 and 0.05, respectively. After determining the degree of freedom, and the level of a significance test, the critical value of the T-test can be obtained using the critical table. The critical table of the t-test shows that $t_5(0.05) = 2.571$; when $|t| \geq |t_5(0.05)|$, the influence factor has a significant effect on multifractal dimensions.

(3) Finally, the influencing factors are quantitatively analyzed. The larger the absolute value of the influencing weight coefficient is, the greater the prestige of the factor on the fractal dimension is, and vice versa.

As can be observed, the correlation effect of the multivariate linear regression model is excellent. On the one hand, for adsorption pores, the total pore area, and the contents of TOC and clay minerals have significant effects on D_A, while the average pore size has no apparent effect. On the other hand, for seepage pores, only the average pore size has a significant effect on the D_S, while the total pore area, the contents of TOC and clay mineral composition have no apparent effect, which confirms the above analysis. The multivariate linear regression model of fractal dimension can be expressed as follows:

$$\begin{aligned} D_A &= 1.648 + 0.413S + 0.578C_T - 0.390C_c \\ D_S &= 3.148 - 1.154r \end{aligned} \quad (12)$$

5. Conclusions

In this paper, the pore structure and fractal features of three typical coal-measure sedimentary rocks from the Daqiang and Jiahe Coal Mines in China were investigated using MIP and NMR experiments. The following conclusions were obtained:

(1) The investigated samples are dominated by clay minerals and quartz, with TOC contents ranging from 0.03% to 10.81%. The main composition of clay minerals is kaolinite and chlorite.

(2) The pore structure features of the investigated samples reveal obvious deviations. All the PSD curves are unimodal distributions. The sandstone (SS-1), mudstone, and shale

are mainly with nanopores of 0.01–1 μm, while the sandstone (SS-2) is dominated by mesopores and macropores of 1–100 μm.

(3) The pore structures of the investigated samples show prominent multipartite characteristics using MIP and NMR tests. Multifractal dimensions can better characterize the heterogeneity of rock samples, in which D_A reflects the surface structure of micropores, while D_S represents the pore structure of macropores.

(4) Multifractal dimensions are affected by many factors, in which D_A is greatly influenced by the pore surface features and mineral components and D_S by average pore diameters. Moreover, the multivariate linear regression model of adsorption pores and seepage pores were established, respectively, which has a better correlation effect on the multifractal dimensions.

Author Contributions: Conceptualization, N.Z.; Methodology, S.W.; Software, X.X.; Validation, H.W.; Resources, X.S. and M.H.; Writing—original draft, S.W. All authors have read and agreed to the published version of the manuscript.

Funding: Funding for this study was provided by the National Natural Science Foundation of China (42277195), the Innovation Fund Research of China University of Mining & Technology, Beijing (SKLGDUEK202218), the Fundamental Research Funds for the Central Universities of China (2021YJSSB10), and the Undergraduate Innovation Program of China University of Mining & Technology, Beijing (C202006968).

Data Availability Statement: Not applicable.

Conflicts of Interest: The authors declare no conflict of interest.

References

1. Zou, C.N.; Yang, Z.; Tao, S.Z.; Yuan, X.J.; Zhu, R.K.; Hou, L.H.; Wu, S.T.; Sun, L.; Zhang, G.S.; Bai, B.; et al. Continuous hydrocarbon accumulation over a large area as a distinguishing characteristic of unconventional petroleum: The Ordos Basin, North-Central China. *Earth-Sci. Rev.* **2013**, *126*, 358–369. [CrossRef]
2. Wang, Y.; Liu, L.; Cheng, H. Gas Adsorption Characterization of Pore Structure of Organic-rich Shale: Insights into Contribution of Organic Matter to Shale Pore Network. *Nat. Resour. Res.* **2021**, *30*, 2377–2395. [CrossRef]
3. Xu, S.; Hu, E.; Li, X.; Xu, Y. Quantitative Analysis of Pore Structure and Its Impact on Methane Adsorption Capacity of Coal. *Nat. Resour. Res.* **2020**, *30*, 605–620. [CrossRef]
4. Loucks, R.G.; Reed, R.M.; Ruppel, S.C.; Hammes, U. Spectrum of pore types and networks in mudrocks and a descriptive classification for matrix-related mudrock pores. *Aapg. Bull.* **2012**, *96*, 1071–1098. [CrossRef]
5. Clarkson, C.R.; Solano, N.; Bustin, R.M.; Bustin, A.M.M.; Chalmers, G.R.L.; He, L.; Melnichenko, Y.B.; Radliński, A.P.; Blach, T.P. Pore structure characterization of North American shale gas reservoirs using USANS/SANS, gas adsorption, and mercury intrusion. *Fuel* **2013**, *103*, 606–616. [CrossRef]
6. Jiang, J.; Yang, W.; Cheng, Y.; Zhao, K.; Zheng, S. Pore structure characterization of coal particles via MIP, N_2 and CO_2 adsorption: Effect of coalification on nanopores evolution. *Powder Technol.* **2019**, *354*, 136–148. [CrossRef]
7. Yang, X.; Guo, S. Comparative analysis of shale pore size characterization methods. *Pet. Sci. Technol.* **2020**, *38*, 793–799. [CrossRef]
8. Shi, X.; Xu, H.; Che, M.; Xiao, C.; Ni, H.; Gao, Q. Investigations of fracture behavior and pore structure change in pulse fracturing for cement block. *Int. J. Rock. Mech. Min. Sci.* **2023**, *166*, 105366. [CrossRef]
9. Zhao, Y.; Sun, Y.; Yuan, L.; Xu, Q. Impact of nanopore structure on coal strength: A study based on synchrotron radiation nano-CT. *Results Phys.* **2020**, *17*, 103029. [CrossRef]
10. Liu, S.; Huang, Z. Exploration of microstructure characteristics and mechanical behaviors of thermal-damaged argillaceous sandstone via LF-NMR and μ-CT technologies. *Geomech. Geophys. Geo* **2023**, *9*, 27. [CrossRef]
11. Zhang, N.; Zhao, F.; Guo, P.; Li, J.; Gong, W.; Guo, Z.; Sun, X. Nanoscale Pore Structure Characterization and Permeability of Mudrocks and Fine-Grained Sandstones in Coal Reservoirs by Scanning Electron Microscopy, Mercury Intrusion Porosimetry, and Low-Field Nuclear Magnetic Resonance. *Geofluids* **2018**, *2018*, 2905141. [CrossRef]
12. He, J.; Ding, W.; Li, A.; Sun, Y.; Dai, P.; Yin, S.; Chen, E.; Gu, Y. Quantitative microporosity evaluation using mercury injection and digital image analysis in tight carbonate rocks: A case study from the Ordovician in the Tazhong Palaeouplift, Tarim Basin, NW China. *J. Nat. Gas. Sci. Eng.* **2016**, *34*, 627–644. [CrossRef]
13. Yang, R.; He, S.; Yi, J.; Hu, Q. Nano-scale pore structure and fractal dimension of organic-rich Wufeng-Longmaxi shale from Jiaoshiba area, Sichuan Basin: Investigations using FE-SEM, gas adsorption and helium pycnometry. *Mar. Pet. Geol.* **2016**, *70*, 27–45. [CrossRef]

14. Fu, H.; Yan, D.; Yao, C.; Su, X.; Wang, X.; Wang, H.; Li, Y. Pore Structure and Multi-Scale Fractal Characteristics of Adsorbed Pores in Marine Shale: A Case Study of the Lower Silurian Longmaxi Shale in the Sichuan Basin, China. *J. Earth Sci.* **2022**, *33*, 1278–1290. [CrossRef]
15. Song, Z.; Liu, G.; Yang, W.; Zou, H.; Sun, M.; Wang, X. Multi-fractal distribution analysis for pore structure characterization of tight sandstone—A case study of the Upper Paleozoic tight formations in the Longdong District, Ordos Basin. *Mar. Pet. Geol.* **2018**, *92*, 842–854. [CrossRef]
16. Wang, T.; Tian, F.; Deng, Z.; Hu, H.; Xie, Z.; Liu, D. The Pore Structure of Marine to Continental Transitional Shales in the Permian Shanxi Formation on the East Margin of the Ordos Basin, China. *Geofluids* **2022**, *2022*, 5601862. [CrossRef]
17. Zhang, N.; Wang, S.; Zhao, F.; Sun, X.; He, M. Characterization of the Pore Structure and Fluid Movability of Coal-Measure Sedimentary Rocks by Nuclear Magnetic Resonance (NMR). *ACS Omega* **2021**, *6*, 22831–22839. [CrossRef]
18. Wu, B.; Xie, R.; Wang, X.; Wang, T.; Yue, W. Characterization of pore structure of tight sandstone reservoirs based on fractal analysis of NMR echo data. *J. Nat. Gas Sci. Eng.* **2020**, *81*, 103483. [CrossRef]
19. Li, Z.; Shen, X.; Qi, Z.; Hu, R. Study on the pore structure and fractal characteristics of marine and continental shale based on mercury porosimetry, N2 adsorption and NMR methods. *J. Nat. Gas Sci. Eng.* **2018**, *53*, 12–21. [CrossRef]
20. Al-Yaseri, A.Z.; Lebedev, M.; Vogt, S.J.; Johns, M.L.; Barifcani, A.; Iglauer, S. Pore-scale analysis of formation damage in Bentheimer sandstone with in-situ NMR and micro-computed tomography experiments. *J. Pet. Sci. Eng.* **2015**, *129*, 48–57. [CrossRef]
21. Xie, R.; Wu, Y.; Liu, K.; Liu, M.; Xiao, L. De-noising methods for NMR logging echo signals based on wavelet transform. *J. Geophys. Eng.* **2014**, *11*, 035003. [CrossRef]
22. Xie, W.; Yin, Q.; Zeng, J.; Wang, G.; Feng, C.; Zhang, P. Fractal-Based Approaches to Pore Structure Investigation and Water Saturation Prediction from NMR Measurements: A Case Study of the Gas-Bearing Tight Sandstone Reservoir in Nanpu Sag. *Fractal Fract.* **2023**, *7*, 273. [CrossRef]
23. Guo, X.; Huang, Z.; Zhao, L.; Han, W.; Ding, C.; Sun, X.; Yan, R.; Zhang, T.; Yang, X.; Wang, R. Pore structure and multi-fractal analysis of tight sandstone using MIP, NMR and NMRC methods: A case study from the Kuqa depression, China. *J. Pet. Sci. Eng.* **2019**, *178*, 544–558. [CrossRef]
24. Wang, G.; Han, D.; Qin, X.; Liu, Z.; Liu, J. A comprehensive method for studying pore structure and seepage characteristics of coal mass based on 3D CT reconstruction and NMR. *Fuel* **2020**, *281*, 118735. [CrossRef]
25. Wang, J.; Cao, Y.; Liu, K.; Gao, Y.; Qin, Z. Fractal characteristics of the pore structures of fine-grained, mixed sedimentary rocks from the Jimsar Sag, Junggar Basin: Implications for lacustrine tight oil accumulations. *J. Pet. Sci. Eng.* **2019**, *182*, 106363. [CrossRef]
26. Ramia, M.E.; Martín, C.A. Sedimentary rock porosity studied by electromagnetic techniques: Nuclear magnetic resonance and dielectric permittivity. *Appl. Phys. A* **2014**, *118*, 769–777. [CrossRef]
27. Gao, H.; Li, H. Determination of movable fluid percentage and movable fluid porosity in ultra-low permeability sandstone using nuclear magnetic resonance (NMR) technique. *J. Pet. Sci. Eng.* **2015**, *133*, 258–267. [CrossRef]
28. Li, X.; Kang, Y.; Haghighi, M. Investigation of pore size distributions of coals with different structures by nuclear magnetic resonance (NMR) and mercury intrusion porosimetry (MIP). *Measurement* **2018**, *116*, 122–128. [CrossRef]
29. Wang, F.; Yang, K.; Cai, J. Fractal characterization of tight oil reservoir pore structure using nuclear magnetic resonance and mercury intrusion porosimetry. *Fractals* **2018**, *26*, 1840017. [CrossRef]
30. Wang, F.; Yang, K.; You, J.; Lei, X. Analysis of pore size distribution and fractal dimension in tight sandstone with mercury intrusion porosimetry. *Results Phys.* **2019**, *13*, 102283. [CrossRef]
31. Yan, J.; Zhang, S.; Wang, J.; Hu, Q.; Wang, M.; Chao, J. Applying Fractal Theory to Characterize the Pore Structure of Lacustrine Shale from the Zhanhua Depression in Bohai Bay Basin, Eastern China. *Energy Fuels* **2018**, *32*, 7539–7556. [CrossRef]
32. Lai, J.; Wang, G. Fractal analysis of tight gas sandstones using high-pressure mercury intrusion techniques. *J. Nat. Gas Sci. Eng.* **2015**, *24*, 185–196. [CrossRef]
33. Turlapati, V.Y.; Prusty, B.K.; Bakshi, T. Detailed Pore Structure Study of Damodar Valley and Upper Assam Basin Shales Using Fractal Analysis. *Energy Fuels* **2020**, *34*, 14001–14011. [CrossRef]
34. Zhang, J.; Li, X.; Wei, Q.; Sun, K.; Zhang, G.; Wang, F. Characterization of Full-Sized Pore Structure and Fractal Characteristics of Marine–Continental Transitional Longtan Formation Shale of Sichuan Basin, South China. *Energy Fuels* **2017**, *31*, 10490–10504. [CrossRef]
35. Zhou, L.; Kang, Z. Fractal characterization of pores in shales using NMR: A case study from the Lower Cambrian Niutitang Formation in the Middle Yangtze Platform, Southwest China. *J. Nat. Gas Sci. Eng.* **2016**, *35*, 860–872. [CrossRef]
36. Yao, Y.; Liu, D.; Che, Y.; Tang, D.; Tang, S.; Huang, W. Petrophysical characterization of coals by low-field nuclear magnetic resonance (NMR). *Fuel* **2010**, *89*, 1371–1380. [CrossRef]
37. Fan, X.; Wang, G.; Li, Y.; Dai, Q.; Linghu, S.; Duan, C.; Zhang, C.; Zhang, F. Pore structure evaluation of tight reservoirs in the mixed siliciclastic-carbonate sediments using fractal analysis of NMR experiments and logs. *Mar. Pet. Geol.* **2019**, *109*, 484–493. [CrossRef]
38. Zhao, Y.; Zhu, G.; Dong, Y.; Danesh, N.N.; Chen, Z.; Zhang, T. Comparison of low-field NMR and microfocus X-ray computed tomography in fractal characterization of pores in artificial cores. *Fuel* **2017**, *210*, 217–226. [CrossRef]
39. *ISO/WD 19990:2023*; Natural Stones—Determination of Water Absorption, Density, Porosity, and Bulk Specific Gravity. International Organization for Standardization: Geneva, Switzerland, 2023.

40. *ISO 10370:2014*; Petroleum Products—Determination of Carbon Residue—Micro Method. International Organization for Standardization: Geneva, Switzerland, 2014.
41. *ISO 14689:2017*; Geotechnical Investigation and Testing—Identification, Description and Classification of Rock. Organization for Standardization: Geneva, Switzerland, 2017.
42. *ISO 15901-1:2016*; Evaluation of Pore Size Distribution and Porosity of Solid Materials by Mercury Porosimetry and Gas Adsorption—Part 1: Mercury Porosimetry. International Organization for Standardization: Geneva, Switzerland, 2016.
43. Lai, J.; Wang, G.; Fan, Z.; Chen, J.; Wang, S.; Zhou, Z.; Fan, X. Insight into the Pore Structure of Tight Sandstones Using NMR and HPMI Measurements. *Energy Fuels* **2016**, *30*, 10200–10214. [CrossRef]
44. Zhang, P.; Lu, S.; Li, J.; Chen, C.; Xue, H.; Zhang, J. Petrophysical characterization of oil-bearing shales by low-field nuclear magnetic resonance (NMR). *Mar. Pet. Geol.* **2018**, *89*, 775–785. [CrossRef]
45. *ASTM E2977-14*; Standard Practice For Measuring and Reporting Performance Of Fourier-Transform Nuclear Magnetic Resonance (FT-NMR) Spectrometers For Liquid Samples. American Society for Testing and Materials: West Conshohocken, PA, USA, 2014.
46. Cheng, M.; Li, C.; Zhou, L.; Feng, L.; Algeo, T.J.; Zhang, F.; Romaniello, S.; Jin, C.; Ling, H.; Jiang, S. Transient deep-water oxygenation in the early Cambrian Nanhua Basin, South China. *Geochim. Cosmochim. Acta* **2017**, *210*, 42–58. [CrossRef]
47. Ge, X.; Fan, Y.; Zhu, X.; Li, R. Determination of nuclear magnetic resonance T-2 cutoff value based on multifractal theory—An application in sandstone with complex pore structure. *Geophysics* **2015**, *80*, D11–D21. [CrossRef]
48. Li, J.; Wang, S.; Lu, S.; Zhang, P.; Cai, J.; Zhao, J.; Li, W. Microdistribution and mobility of water in gas shale: A theoretical and experimental study. *Mar. Pet. Geol.* **2019**, *102*, 496–507. [CrossRef]
49. Shao, X.; Pang, X.; Li, H.; Zhang, X. Fractal Analysis of Pore Network in Tight Gas Sandstones Using NMR Method: A Case Study from the Ordos Basin, China. *Energy Fuels* **2017**, *31*, 10358–10368. [CrossRef]
50. Ji, W.; Song, Y.; Jiang, Z.; Meng, M.; Liu, Q.; Chen, L.; Wang, P.; Gao, F.; Huang, H. Fractal characteristics of nano-pores in the Lower Silurian Longmaxi shales from the Upper Yangtze Platform, south China. *Mar. Pet. Geol.* **2016**, *78*, 88–98. [CrossRef]